Macromolecules

ARTICLE

pubs.acs.org/Macromolecules

Poly(vinyl alcohol) Nanocomposites with Nanodiamond

Seira Morimune,[†] Masaru Kotera,[†] Takashi Nishino,[*,†] Kimiya Goto,[‡] and Katsuhiko Hata[‡]

[†]Department of Chemical Science and Engineering, Graduate School of Engineering, Kobe University, Rokko, Nada, Kobe 657-8501, Japan

[‡]Bando Chem. Ind., Ltd., Minatojima-Minami, Chuo, Kobe 650-0047, Japan

Supporting Information

ABSTRACT: Carbon-based nanomaterials, such as carbon nanotubes, are well-known for their unique physical properties. They have attracted interest as reinforcing fillers because of their superb mechanical properties (Young's modulus ≥1 TPa and tensile strength = 100−150 GPa). However, the success of the reinforcement has been limited because of their tendency to form agglomerates in polymer matrices. We report the excellent reinforcement properties of polymer nanocomposites by the incorporation of nanodiamond (ND). ND has been expected to offer polymer nanocomposites optimal properties because of its smooth surface and excellent optical, mechanical, and thermal properties, which can approach the values of single diamond crystal. We prepared poly(vinyl alcohol) (PVA)/ND nanocomposites by a simple casting method from aqueous medium and achieved the high dispersibility of ND in the PVA matrices. The resulting nanocomposites had excellent properties derived both from ND and PVA. The Young's modulus of the nanocomposites in particular increased 2.5 times compared with that of PVA film with only 1 wt % ND loading. For the thermal properties, the thermal conductivity of the nanocomposites increased dramatically, much above the calculated values, especially at a low content of ND. Furthermore, it was revealed that PVA/ND nanocomposites remained high transparency of PVA even if ND particles were imparted. We anticipate that ND will be able to compete as a nanofiller against conventional carbon-based nanofillers for polymer composites, and it is possible their reinforcement properties will be extended in the future.

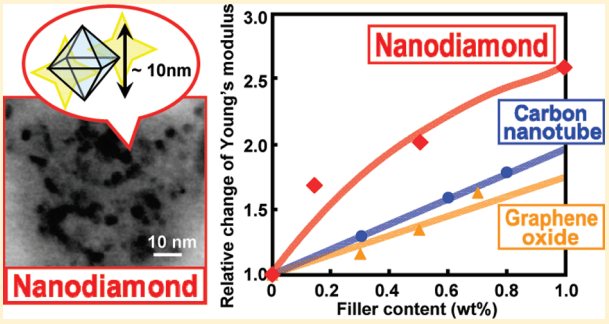

1. INTRODUCTION

Polymer nanocomposites have attracted much attention not only in scientific fields but also in industrial applications due to the excellent abilities of nano-sized fillers. The first major success with nanocomposites was the nylon-6/clay nanocomposite (Toyota Central R&D Laboratories., Inc.) with significant improvements in the Young's modulus and the tensile strength.[1] Since then, works on nanocomposites have been conducted on a wide variety of combinations together with thermoplastics (styrenics, polyolefins) and thermosetting polymers (epoxy resins and phenolics) with various fillers, such as layered silicates and carbon-based nanomaterials. Nanocomposites have been reported to provide remarkable improvements in materials properties, including mechanical, thermal, and barrier properties, compared with those of polymer itself and micro-sized fillers composites.[2,3]

Carbon-based nanomaterials, such as carbon nanotubes, are well-known for their incredibly high mechanical properties (Young's modulus ≥ 1 TPa and tensile strength = 100−150 GPa), and they have attracted interest as reinforcing fillers for polymer nanocomposites.[4−7] However, the success of the reinforcement has been limited because of their tendency to form agglomerates in polymer matrices.[8,9] In recent years, nanodiamond (ND) has been produced by several procedures, such as by explosion, and it has been exploited in some fields of nanotechnology.[10−12] Diamond is well-known for its excellent properties, such as the highest bulk modulus, the highest thermal conductivity, high wear resistance, chemical inertness, and good electrical insulating properties. Therefore, ND has been expected to offer polymer nanocomposites optimal properties due to its own excellent properties, which can approach the values of single-crystal diamond.[13]

In this study, we selected poly(vinyl alcohol) (PVA), a water-soluble and biodegradable polymer, as a polymer matrix. PVA has been widely used not only in scientific fields but also in industrial fields.[14,15] In addition, PVA has been extensively studied as a matrix for polymer composites, and its high performance has been often reported.[8,16−18] We prepared PVA/ND nanocomposites by simple casting from an aqueous suspension, and we investigated the structure and properties of the nanocomposites.

2. EXPERIMENTAL SECTION

2.1. Materials. PVA was supplied from Nippon Synthetic Chemical Industry Co., Ltd., with its commercial name "Gohsenol NH-18"; the degree of polymerization is 1800, and the degree of saponification is

Received: January 25, 2011
Revised: March 31, 2011
Published: May 03, 2011

more than 99%. ND aqueous suspension was supplied from Bando Chem. Ind.; the ND content is 2.75 wt %. ND powder was synthesized by the detonation of explosive compounds, including TNT (2-methyl-1,3,5-trinitrobenzene) and RDX (hexahydro-1,3,5-trinitro-1,3,5-triazine), under an inert atmosphere. The detonation soot was purified by oxidation with the strong acids, such as permanganic acid, nitric acid, and sulfuric acid, followed by annealing. After rinsing, the ND powder was dispersed in water by wet milling process in bead mill. All the materials were used as received.

2.2. Sample Preparation. The PVA/ND nanocomposites were prepared by a simple casting method. ND aqueous suspension was ultrasonicated for 1 h. PVA powder was then added to the ND aqueous suspension. The suspension was continuously stirred at 90 °C for 3 h to dissolve PVA. The ND content (0−5 wt % vs PVA) was controlled by the amount of PVA added. The PVA/ND aqueous suspension was cast into a Petri dish and dried at room temperature and then in a vacuum at 40 °C for 48 h. The film thickness was controlled at 100 μm.

2.3. Characterization. The ND particles and the PVA/ND nanocomposite were observed using a field emission scanning electron microscope (FE-SEM) (JEOL, JSM-6700F) at an accelerating voltage of 10 kV. Pt/Pd was deposited on the sample surface prior to observation. Fourier transform infrared spectrum (FTIR) of ND was recorded on a FTIR spectrophotometer (Perkin-Elmer, Spectrum GX FT-IR System I-KS) using the KBr method. The resolution was 2 cm^{-1}. X-ray photoelectron spectroscopy (XPS) measurements were carried out with an ESCA-3400 spectrometer (Shimadzu Co.). The sample surface was irradiated by Mg Kα radiation, generated at 8 kV and 30 mA. X-ray diffraction (XRD) was performed using an X-ray diffractometer (Rigaku, RINT2100) equipped with Ni-filtered Cu Kα radiation. The X-ray beam was operated at 40 kV and 20 mA. The 2θ scan data were collected at 0.02° intervals at a scanning speed of 1.0°/min.

Tensile properties were determined using a tensile tester, Autograph AGS-1kND (Shimadzu Co.); the initial length of the specimen was 20 mm, and the extension rate was 2 mm/min. The number of tested specimens was more than ten. The toughness (K) was determined as the area surrounded by the stress (σ)−strain (ε) curve. It was calculated using the equation

$$K = \int_{\varepsilon=0}^{\varepsilon=\varepsilon_{max}} \sigma \, d\varepsilon/d \quad (J/g) \tag{1}$$

where σ is the stress (Pa), ε the strain (%), and d the density (m^3/g).

Dynamic mechanical analysis was performed with a dynamic mechanical analyzer, DVA-220S (ITK Co., Ltd.), under nitrogen flow. A heating rate was 6 °C/min, and a frequency of 10 Hz was employed. Humidity dependence of the storage modulus was also measured by changing the relative humidity (RH) with 1% RH/min at 60 °C.

The melting point (T_m) was measured by a differential scanning calorimeter (DSC) (Seiko Instruments Inc., DSC-220CU). A heating rate of 10 °C/min was used under nitrogen flow. The thermal decomposition temperature (T_d), defined as a temperature of 5 wt % thermal weight loss, was determined by a thermogravimeter (TG) (Seiko Instruments Inc., TG/DTA-220CU). A heating rate of 10 °C/min was employed under nitrogen flow. Thermal conductivity measurements were carried out on a series of PVA/ND nanocomposites as a function of the ND content. The measurements were conducted using a precise and prompt thermal property measuring instrument (Kato Tech Co., Ltd., KES-F7). The thermal conductivity λ (W/(m K)) can be obtained from the equation

$$\lambda = \frac{WD}{A\Delta T} \tag{2}$$

where W is the thermal loss of heat plate (W), D the thickness of sample (m), A the area of heat plate (m^2), and ΔT the temperature difference of sample (K). Thermal expansion behavior was measured using TMA/SS-120CU (Seiko Instruments, Co.). A heating rate was 10 °C/min under nitrogen flow. The instrument was operated in tension mode under the stress of 1 MPa.

The ultraviolet−visible (UV−vis) spectra were observed at room temperature using a UV−vis spectrophotometer (Hitachi Ltd., U-2000) at a wavelength scan rate of 400 nm/min.

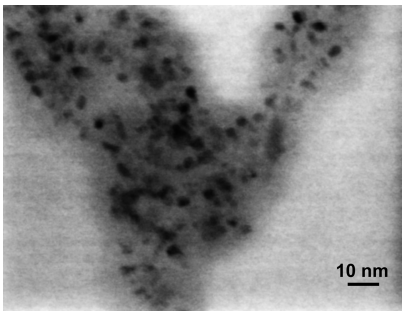

Figure 1. FE-SEM photograph of ND particles.

3. RESULTS AND DISCUSSION

3.1. Characterization. Figure 1 shows field emission scanning electron microscopy (FE-SEM) photographs of the ND particles. The size of the primary ND particles was found to be up to 10 nm. The smokelike structure was also observed to surround the ND particles; this was found to contain graphitic carbons.[19−21]

Figure 2a shows the Fourier transform infrared (FTIR) spectrum of the ND particles. Absorption bands around 2830−2960 and 1300−1400 cm^{-1} can be assigned to C−H stretching and deformation vibration of alkyl group, respectively.[22] The band at 1628 cm^{-1} can be assigned to stretching vibration of aromatic sp^2 carbon bond which can be related to graphite around the ND particles. The spectrum revealed another bands from oxygen containing functional groups, at 1759 cm^{-1} (C═O stretching vibration in carbonyl, carboxyl groups) and around 1100−1200 cm^{-1} (C−O stretching vibration in ethers).[23−25] Strong absorption bands assigned as hydroxyl groups appeared in the spectra area of 3300−3500 cm^{-1} (O−H stretching vibration) and 1620−1630 cm^{-1} (O−H bending vibration).[23,24] These are originated from the hydroxyl groups of adsorbed water on the particles in air because there exist many dangling bonds on the diamond structured surface of the ND particles.[25] In addition, a process of "self-functionalization" occurred during the preparation of the ND particles, acquiring "functional cover" including these oxygen-containing functional groups.[26] The spectra area of 1600−1650 cm^{-1} is most likely to be connected with several band superposition including asymmetric O−N vibration of R−O−NO_2 groups. Usually the ND particles were produced by explosion using trinitrotoluene and hexogen mixture.[27] Thus, the observed nitrogen may be the residue in a process of producing the ND particles.

Figure 2b−d shows (b) X-ray photoelectron spectroscopy (XPS) wide spectrum and the table of XPS analysis as well as (c) C 1s and (d) O 1s spectra of the ND particles. Figure 2b represents the sharp peaks of oxygen and carbon on the ND surface. From the table in the top right of Figure 2b, the ND particles contain 15.9% of O, which can be related to the absorbed H_2O and oxygen containing functional groups. Judging from the results of XPS as well as that of FTIR

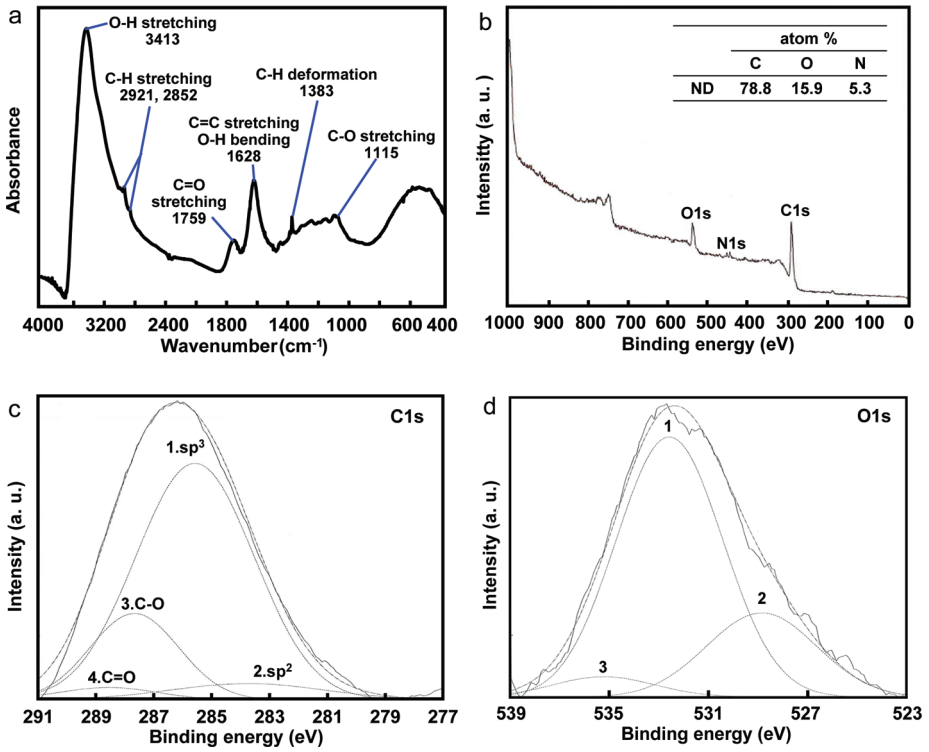

Figure 2. (a) FT-IR spectrum of ND particles, (b) XPS spectrum and XPS analysis table of ND particles, (c) C 1s XPS spectrum of ND particles, and (d) O 1s XPS spectrum of ND particles.

Scheme 1. Schematic Illustration of the Interaction between PVA and ND Particles

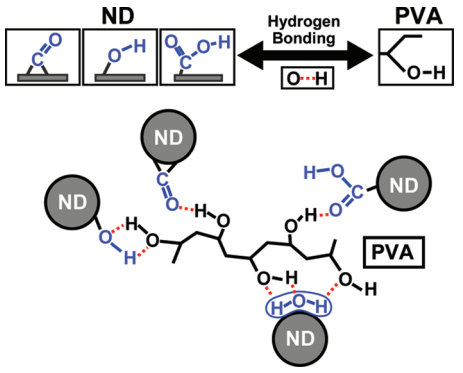

(Figure 2a), carboxyl, carbonyl, and ether groups exist together with hydroxyl groups. In addition, we could observe the small peak at around 400 eV, which indicates the existence of nitrogen. As described above, nitrogen seems to be produced during the ND production process. From Figure 2c, the C 1s spectra can be curve resolved into four peaks including the most intense peak at 285.6 eV (peak 1); the bulk diamond components of sp^3 carbon and alkyl group, the peak at 283.4 eV (peak 2); graphitic carbon species of sp^2 carbon, the peak at 287.7 eV (peak 3); ethers, and the peak at 288.6 eV (peak 4); carbonyl groups. The O 1s spectrum deconvolution reveals that the spectrum can be fit with three maxima. The peak at 532.6 eV (peak 1) can be related to carboxyl, carbonyl, and ethers groups. The other two peaks (peaks 2 and 3) may possibly attribute to H_2O and oxygen.[28]

As described above, the oxygen-containing functional groups on the surface of the ND particles are considered to contribute not only to the good dispersion of the ND particles into aqueous medium but also to the strong interaction, including hydrogen bonding, between ND and PVA (Scheme 1). Korobov et al.[29] reported that the nanophase of water was absorbed on the surface of the ND particles has a huge impact on the dispersibility of ND.

The FE-SEM photographs of the cross section of the PVA/ND nanocomposite with 5 wt % ND loading is shown in Figure 3a. The ND particles were almost well dispersed in PVA matrix. However, small agglomerates 100−200 nm in size could be observed, as shown in the top-right corner of the figure. These agglomerates can serve as thermally conducting channels. The results of thermal conductivity measurements are shown below.

Figure 3b shows the X-ray diffraction (XRD) profiles of the PVA film, the PVA/ND nanocomposites, and the ND particles. The diffraction peaks assigned as 111 and 220 reflections of diamond structure were observed clearly for the ND particles at $2\theta = 43.9°$ and 75.3°, respectively. These indicate that the ND particles possess three-dimensional diamond structure even at a size of no more than 10 nm. In the profiles of the PVA/ND nanocomposites with ND contents over 5 wt %, the 111 reflection also overlapped with the 202 reflection of PVA. From the profile, the crystallinity (X_c) of PVA was determined to be 28%. The X_c of the nanocomposites increased to 34% and 36% with 1 and 5 wt % ND loading, respectively. Similarly, for the annealed samples, the X_c value also increased by the incorporation of the ND particles (Figure S1).

3.2. Mechanical Properties. Figure 4a shows the stress (σ)−strain (ε) curves of the PVA film and the PVA/ND nanocomposites with different ND contents. The PVA film showed the

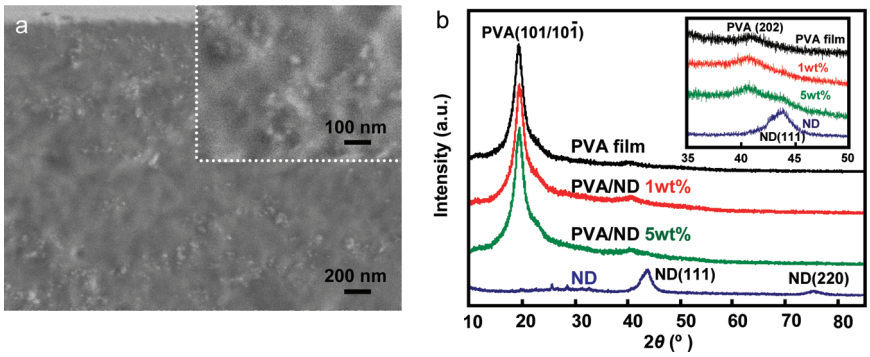

Figure 3. (a) FE-SEM photographs of the cross section of a PVA/ND nanocomposite with 5 wt % ND loading. (b) X-ray diffraction profiles of PVA film, PVA/ND nanocomposites, and ND particles.

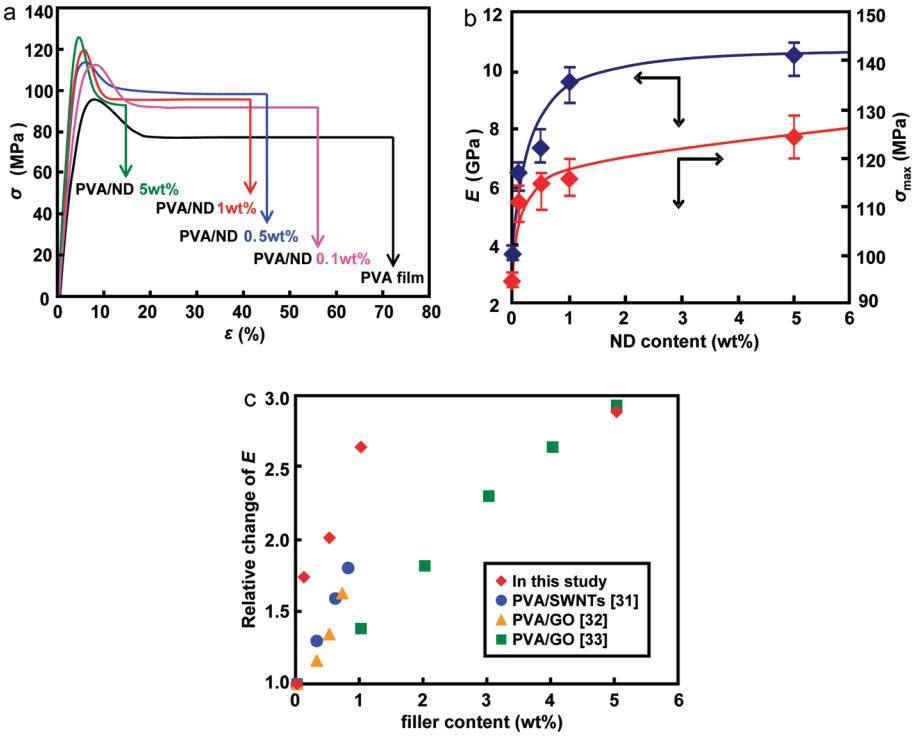

Figure 4. (a) Stress (σ)−strain (ε) curves of as-cast PVA film and PVA/ND nanocomposites. (b) Relationships between Young's modulus (E), tensile strength (σ_{max}), and ND content of PVA/ND nanocomposites. (c) Relationship between relative change of the Young's modulus (E) versus that of PVA and filler content of PVA/carbon-based nanomaterial (ND, SWNTs,[31] GO,[32,33]) composites.

typical $\sigma-\varepsilon$ curve for a conventional polymer film with yielding. The tensile strength (σ_{max}) in these curves, equal to the yielding stress, and the Young's modulus (E) increased drastically with the ND content.

Figure 4b shows the relationships between the E, the σ_{max}, and the ND content of the PVA/ND nanocomposites. The E of the nanocomposite was found to be 150% higher than that of the PVA film and reached 9.7 GPa with only 1 wt % ND loading. The σ_{max} increased by 30% (at 5 wt % ND loading) compared with that of the PVA film (see also Table 1). The remarkable increase in E and σ_{max} were also observed in the annealed samples (Figure S2a,b). This high mechanical performance implies that a sufficiently small size and good dispersion of ND particles achieved a large interfacial area, causing the strong interaction between PVA and ND to increase. Besides the excellent reinforcement effect of the ND particles, the high E value of the nanocomposites also attributed to the increase of the X_c of the PVA matrix. Therefore, the outstanding mechanical properties of ND were imparted to the nanocomposites effectively.

Diamond is known for its extremely high E value, above 1000 GPa. The incorporation of diamond particles in PVA matrix as a filler is expected to increase the E of the composite remarkably. As a first approximation, this increase can be predicted using a simple rule of mixture with the equation

$$E_c = E_f V_f + E_m(1 - V_f) \quad (3)$$

where E_c, E_f, and E_m are the E of the composites, filler, and matrix, respectively, and V_f is the volume fraction of filler. Assuming E_f = 1050 GPa,[30] E_m = 3.7 GPa, and that 1 wt % ND loading

corresponds to $V_f = 0.005$, E_c is estimated to be 8.9 GPa, which is comparable to the observed value (9.7 ± 0.6 GPa).

Figure 4c shows the comparison of the E value with other carbon-based nanomaterial composites reported in the literature. Liu et al.[31] worked on the composites of PVA with single-walled carbon nanotubes (SWNTs), being functionalized the surface with multiple hydroxyl groups in order to overcome the agglomeration of SWNTs in the PVA matrix. They reported that the E value increased from 2.4 to 4.3 GPa with 0.8 wt % SWNTs loading compared with the case of the PVA film (1.8 times). On the other hand, Liang et al.[32] and Xu et al.[33] reported that the E value increased linearly with the incorporation of graphene oxide (GO) in the PVA matrix. Graphene oxide (GO), one of functionalized graphene materials, bears oxygen-containing groups on basal planes and edges of graphene. These groups attach the desired characteristic of water dispersibility to the pristine graphene. Therefore, the nanodispersion in the PVA matrix can be expected. The E value reported by Liang et al. increased from 2.1 to 3.4 GPa (1.6 times) with 0.7 wt % GO loading, and Xu et al. reported an increase from 2.1 to 6.1 GPa (2.9 times) with 5 wt % GO loading, compared with the case of the PVA film. In comparison to those of other composites, the E value of the PVA/ND nanocomposites drastically increased at a low content of ND particles (less than 1 wt %). The PVA/ND nanocomposite achieved an E value of 9.7 GPa with only 1 wt % ND loading, which is the highest value among the examined carbon-based nanomaterial composites. As mentioned above, the nanophase of water was absorbed on the surface of the ND particles, which could not be observed in the other examined carbon-based nanomaterial composites. Accordingly, the absorved water will have a large effect not only on the dispersibility of ND but also on the interaction with the PVA matrix and derive the optimal reinforcement effect of ND.

Table 1. Young's Modulus (E), Tensile Strength (σ_{max}), Strain at Break (ε_{max}), and Toughness (K) of PVA Film and PVA/ND Nanocomposites

	E, GPa	σ_{max}, MPa	ε_{max}, %	K, J/g
PVA	3.7 ± 0.2	95 ± 2.5	72 ± 3.1	43
PVA/ND 0.1 wt %	6.4 ± 0.5	111 ± 4.6	55 ± 8.9	45
PVA/ND 0.5 wt %	7.4 ± 0.6	114 ± 5.2	44 ± 2.1	34
PVA/ND 1 wt %	9.7 ± 0.6	115 ± 5.2	41 ± 5.6	27
PVA/ND 5 wt %	10.6 ± 0.8	124 ± 5.4	16 ± 2.9	11

The reinforcement effect of the ND particles in the wide range of temperature (from −150 to 200 °C) was revealed by dynamic mechanical analysis (DMA). Figure 5a shows the temperature dependence of the storage modulus (E') and the tan δ of the PVA film and the PVA/ND nanocomposites. For the tan δ, the main dispersion, so-called α_a, around 61 °C is assigned as the glass transition (T_g) of the PVA matrix. The peak of this α_a dispersion of the PVA/ND nanocomposite with 1 wt % ND loading shifted to a higher temperature (69 °C) and decreased in intensity compared to that of the PVA film. Similarly, the β dispersion around −5 °C was suppressed by the ND loading. The E' value increased within the entire temperature range when the ND particles were incorporated. In particular, above T_g, the decrease of E' was suppressed and a high E' value was maintained. The reinforcement effect caused by the ND particles is considered to be due to the suppressed motion of the polymer chains in the amorphous phase.[16,34−36] In addition, the PVA/ND nanocomposites maintained a high E' value even under high humidity in the range 15%−90% (Figure 5b). This indicates that the penetration pass of water in the PVA matrix was prolonged by the nanodispersion of the ND particles; thus, the relaxation of the PVA molecular chains was suppressed.

3.3. Thermal Properties. Figure 6a shows the differential scanning calorimetry (DSC) thermograms of the PVA film and the PVA/ND nanocomposites. The endotherm assigned as the melting temperature (T_m) of pure PVA (around 225 °C) was clearly observed in every case. From the DSC curves, an increase in the T_g caused by the incorporation of the ND particles was observed: this is in agreement with the results in Figure 5a. The T_g and the T_m of the PVA film and the PVA/ND nanocomposites are summarized in Table 2. The T_m of the PVA/ND nanocomposites were similar to that of pure PVA. Therefore, as mentioned above, the incorporation of the ND particles had an effect not on the crystalline regions but largely on the amorphous region of the PVA matrix and suppressed the molecular motion.

Figure 6b shows the thermogravimetric (TG) traces of the PVA film and the PVA/ND nanocomposites. The onset temperature of the thermal degradation (T_d) of the PVA/ND nanocomposite with 5 wt % ND loading was about 13 °C higher than that of the PVA film (Table 1). This indicates that the nanodispersion of the ND particles can act as a barrier to hinder the volatile decomposition products throughout the composites; thus, the thermal stability can be improved by the incorporation of the ND particles.[37]

Many theoretical and empirical models of thermal conductivity have been developed to describe the mixing rules of two-phase

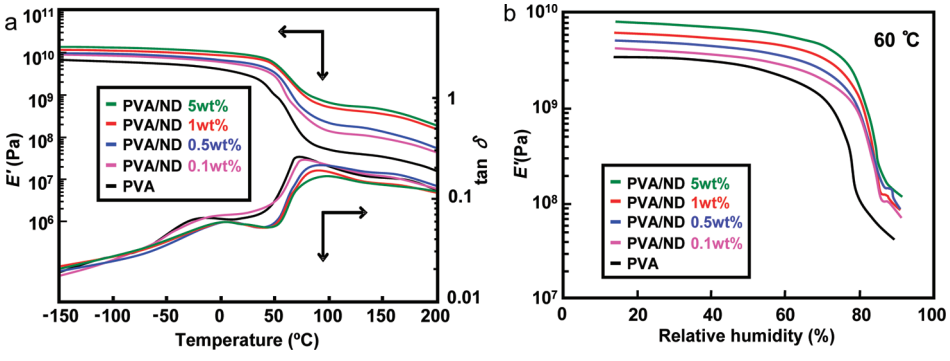

Figure 5. (a) Temperature dependence of the storage modulus (E') and mechanical tan δ of PVA film and PVA/ND nanocomposites. (b) Relative humidity dependence of the storage modulus (E') of PVA film and PVA/ND nanocomposites at 60 °C.

dx.doi.org/10.1021/ma200176r |*Macromolecules* 2011, 44, 4415–4421

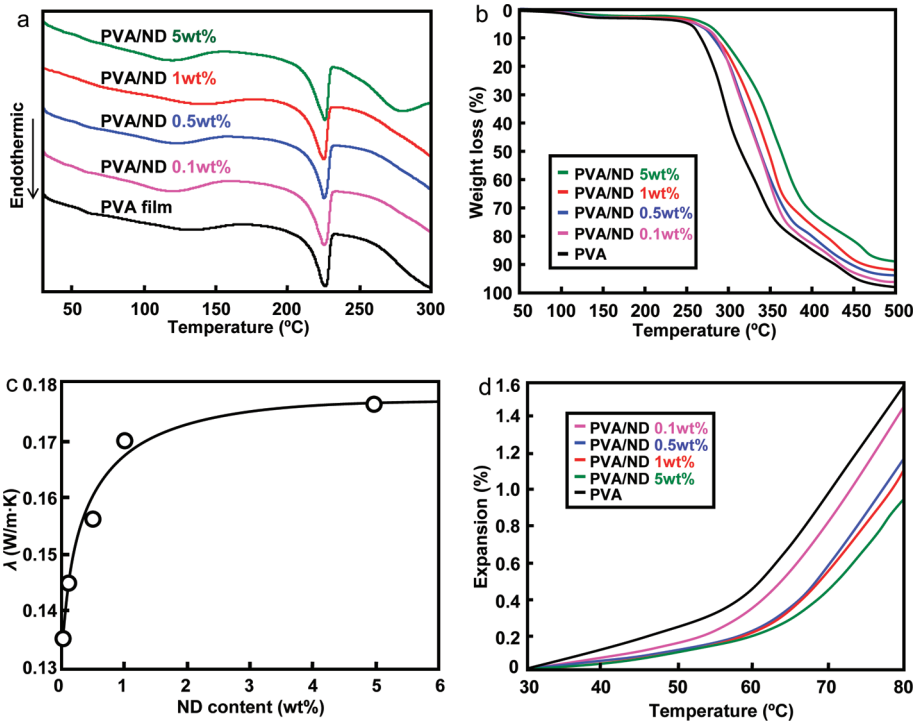

Figure 6. (a) DSC thermograms of PVA film and PVA/ND nanocomposites. (b) Thermogravimetric traces of PVA film and PVA/ND nanocomposites. (c) Relationship between the thermal conductivity (λ) and ND content of as-cast PVA/ND nanocomposites. (d) Thermal expansion behavior of PVA film and PVA/ND nanocomposites under 1 MPa.

Table 2. Thermal Properties of PVA Film and PVA/ND Nanocomposites

	T_g, °C	T_m, °C	T_d, °C	α (40−50 °C), 10^{-5} K^{-1}	α (80−90 °C), 10^{-4} K^{-1}
PVA	62	225	263	8.8	6.9
PVA/ND 0.1 wt %	69	225	269	8.1	6.5
PVA/ND 0.5 wt %	73	226	273	6.6	5.4
PVA/ND 1 wt %	80	226	275	6.3	5.1
PVA/ND 5 wt %	79	226	277	5.7	4.4

composite systems. The most common models to predict thermal conductivity are Maxwell's eq 4 and Bruggeman's eq 5:

$$\lambda_c = \lambda_m \frac{\lambda_f + 2\lambda_m - 2V_f(\lambda_m - \lambda_f)}{\lambda_f + 2\lambda_m + V_f(\lambda_m - \lambda_f)} \quad (4)$$

$$1 - V_f = \frac{\lambda_f - \lambda_c}{\lambda_f - \lambda_m}\left(\frac{\lambda_m}{\lambda_c}\right)^{1/3} \quad (5)$$

where λ_c, λ_m, and λ_f are the effective thermal conductivity of the composites, matrix, and filler particles, respectively, and V_f is the volume fraction of the filler.[38] Assuming λ_m = 0.135 W/(m K) and λ_f = 2000 W/(m K),[39] the λ_c value for the PVA/ND nanocomposite with 1 wt % ND loading gives 0.14 W/(m K) using both eqs 4 and 5.

The relationship between the observed thermal conductivity and the ND content of the PVA/ND nanocomposites is shown in Figure 6c. The thermal conductivity of the nanocomposite with 1 wt % ND loading reached 0.17 W/(m K), which is 25% higher than that of the PVA film and 20% higher than the

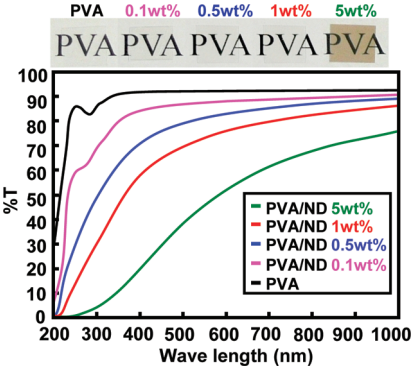

Figure 7. Optical images (top) and UV−vis spectra (bottom) of PVA film and PVA/ND nanocomposites. The film thickness was 100 μm.

calculated values. Thermal conductivity has been explained by the effective medium theory for polymer−nanoparticle composites.[10,40] Because of particle−matrix interfacial thermal resistance, the thermal conductivity of polymer nanocomposites with small spherical particles can be predicted to decrease. In contrast, an increase can be seen for a filler with a high aspect ratio due to sufficiently small interfacial resistance.[41] For the PVA/ND nanocomposite system, however, the thermal conductivity increased in spite of the low aspect ratio of ND. As mentioned above, the ND particles formed some agglomerates within the PVA matrix. This suggests that ND agglomerates served as thermally conducting channels that contribute to the increased overall thermal conductivity of the nanocomposites.[42]

Figure 6d shows the thermal expansion behavior of the PVA film and the PVA/ND nanocomposites. The thermal expansion

was suppressed and the linear thermal expansion coefficient α between 40−50 and 80−90 °C decreased linearly as the loading of ND as shown in Table 1. This indicates that, as described above, the ND particles suppressed the molecular motion of PVA, and then the effective reinforcement was achieved.

3.4. Transparency. Figure 7 shows the ultraviolet−visible (UV−vis) spectra of the PVA film and the PVA/ND nanocomposites. The optical images of the PVA film and the PVA/ND nanocomposites are also superimposed in the top part of the figure. The PVA film exhibited more than 90% transparency across the visible light region. This high transparency enables PVA to be used as a polarizer film in an electric device. Though, with increasing ND content, the transparency decreased, the PVA/ND nanocomposite with lower ND loading achieved a high transparency level close to that of the PVA film. This indicates that the transparency remained high even with 1 wt % ND loading in the visible region.

4. CONCLUSIONS

Nanodispersion of the ND particles in the PVA matrix was achieved by using a simple casting method from aqueous medium. The mechanical properties of the PVA/ND nanocomposites increased remarkably by the incorporation of ND particles. The *E* values of the nanocomposites were comparable to that of calculated up to 1 wt % ND loading. Therefore, the ideal reinforcement effect of ND was revealed. For the thermal properties, the thermal conductivity of the PVA/ND nanocomposite increased drastically even at a low content of ND particles. Furthermore, while possessing the outstanding properties of ND, the nanocomposites maintained the high optical transparency of PVA. Therefore, we created ideal nanocomposites by using ND, which will be able to compete as a nanofiller against conventional carbon-based nanofillers for polymer composites.

■ ASSOCIATED CONTENT

Supporting Information. Sample preparation of the annealed PVA/ND nanocomposites; XRD profiles of annealed PVA film, PVA/ND nanocomposites, and ND particles; stress (σ)−strain (ε) curves and relation between *E*, σ_{max}, and the ND content of annealed PVA/ND nanocomposites; table of the mechanical properties of annealed PVA/ND nanocomposites. This material is available free of charge via the Internet at http://pubs.acs.org.

■ AUTHOR INFORMATION

Corresponding Author

*Tel: 81-78-803-6164. Fax: 81-78-803-6198. E-mail: tnishino@kobe-u.ac.jp.

■ REFERENCES

(1) Kojima, Y.; Usuki, A.; Kawasumi, M.; Okada, A.; Fukushima, Y.; Karauchi, T.; Kamigaito, O. *J. Mater. Res.* **1993**, *8*, 1185.
(2) Sharp, K. G. *Adv. Mater.* **1998**, *10*, 1243.
(3) Fujiyama-Novak, J. H.; Cakmak, M. *Macromolecules* **2008**, *41*, 6444.
(4) Meisha, L. S.; Valery, N. K.; Enrique, V. B. *Chem. Mater.* **2006**, *18*, 906.
(5) Viswanathan, G.; Chakrapani, N.; Yang, H.; Wei, B.; Chung, H.; Cho, K.; Ryu, Y. C.; Ajayan, M. P. *J. Am. Chem. Soc.* **2003**, *125*, 9258.
(6) Stoneham, A. M. *Nature Mater.* **2004**, *3*, 3.
(7) Koziol, K.; Vilatela, J.; Moisala, A.; Motta, M.; Cunniff, P.; Sennett, M.; Windle, A. *Science* **2007**, *318*, 1892.
(8) Wang, Z.; Ciselli, P.; Peijs, T. *Nanotechnology* **2007**, *18*, 1.
(9) Coleman, J. N.; Khan, U.; Gun'ko, Y. K. *Adv. Mater.* **2006**, *18*, 689.
(10) Greiner, R.; Phillips, D. S.; Johnson, J. D.; Volk, A. F. *Nature* **1988**, *333*, 440.
(11) Lam, R.; Chen, M.; Pierstorff, E.; Huang, H.; Osawa, E.; Ho, D. *ACS Nano* **2008**, *2*, 2095.
(12) Behler, K. D.; Stravato, A.; Mochalin, V.; Korneva, G.; Yushin, G.; Gogotsi, Y. *ACS Nano* **2009**, *3*, 363.
(13) Osswald, S.; Yushin, G.; Mochalin, V.; Kucheyev, S. O.; Gogotsi, Y. *J. Am. Chem. Soc.* **2006**, *128*, 11635.
(14) Sakurada, I. *Polyvinyl Alcohol Fibers*; Marcel Dekker: New York, 1985.
(15) Finch, C. A., Ed. *Polyvinyl Alcohol-Developments*; John Wiley and Sons: Chichester, 1992.
(16) Strawhecker, K. E.; Manias, E. *Chem. Mater.* **2000**, *12*, 2943.
(17) Shim, B. S.; Kotov, N. A. *Langmuir* **2005**, *21*, 9381.
(18) Salavagione, H. J.; Gomez, M. A.; Martinez, G. *Macromolecules* **2009**, *42*, 6331.
(19) Hu, S.; Sun, J.; Du, X.; Tian, F.; Jiang, L. *Diamond Relat. Mater.* **2008**, *17*, 142.
(20) Hawelek, L.; Brodka, A.; Dore, J. C.; Honkimaki, V.; Tomita, S.; Burian, A. *Diamond Relat. Mater.* **2008**, *17*, 1186.
(21) Barnard, A. S.; Sternberg, M. *J. Mater. Chem.* **2007**, *17*, 4811.
(22) Zhang, Q.; Naito, K.; Tanaka, Y.; Kagawa, Y. *Macromolecules* **2008**, *41*, 536.
(23) Ozawa, M.; Inaguma, M.; Takahashi, M.; Kataoka, F.; Krüger, A.; Osawa, E. *Adv. Mater.* **2007**, *19*, 1201.
(24) Kuznetsov, V. L. *Carbon* **1991**, *29*, 665.
(25) Lee, J. Y.; Lim, D. P.; Lim, D. S. T. *Composites, Part B* **2007**, *38*, 810.
(26) Bershtein, V. A.; Karabanova, L. V.; Sukhanova, T. E.; Yakushev, P. N.; Egorova, L. M.; Lutsyk, E. D.; Svyatyna, A. V.; Vylegzhanina, M. E. *Polymer* **2008**, *49*, 836.
(27) Mironov, E.; Petrov, E.; Koretz, A. *Diamond Relat. Mater.* **2003**, *12*, 1472.
(28) Patil, A. J.; Vickery, J. L.; Scott, T. B.; Mann, S. *Adv. Mater.* **2009**, *21*, 3159.
(29) Korobov, M. V.; Avramenko, N. V.; Bogachev, A. G.; Rozhkova, N. N.; Osawa, E. *J. Phys. Chem. C* **2007**, *111*, 7330.
(30) Yoder, M. N. In *Diamond Films and Coatings*; Davis, R. F., Ed.; Noyes Publications: Park Ridge, NJ, 1993.
(31) Liu, L. Q.; Barber, A. H.; Nuriel, S.; Wagner, H. D. *Adv. Funct. Mater.* **2005**, *15*, 975.
(32) Liang, J.; Huang, Y.; Zhang, L.; Wang, Y.; Ma, Y.; Guo, T.; Chen, Y. *Adv. Funct. Mater.* **2009**, *19*, 2297.
(33) Xu, Y.; Hong, W.; Bai, H.; Li, C.; Shi, G. *Carbon* **2009**, *47*, 3538.
(34) Lee, C.; Leigh, D. A.; Pritchard, R. G.; Schultz, D.; Teat, S. J.; Timco, G. A.; Winpenny, R. E. P. *Nature* **2009**, *458*, 314.
(35) Wan, C.; Zhang, Y.; Zhang, Y. *Polym. Test.* **2004**, *23*, 299.
(36) Zhou, T. H.; Ruan, W. H.; Rong, M. Z.; Zhang, M. Q.; Mai, Y. L. *Adv. Mater.* **2007**, *19*, 2667.
(37) Podsiadlo, P.; Kaushik, A. K.; Arruda, E. M.; Waas, A. M.; Shim, B. S.; Xu, J.; Nandivada, H.; Pumplin, B. G.; Lahann, J.; Ramamoorthy, A.; Kotov, N. A. *Science* **2007**, *318*, 80.
(38) Wan, J.; Yi, X. S. *Compos. Sci. Technol.* **2004**, *64*, 1623.
(39) Haggerty, S. E. *Science* **1999**, *285*, 851.
(40) Putnam, S. A.; Cahill, D. G.; Ash, B. J.; Schadler, L. S. *J. Appl. Phys.* **2003**, *94*, 6785.
(41) Nan, C. W.; Birringer, R.; Clarke, D. R.; Gleiter, H. *J. Appl. Phys.* **1997**, *81*, 6692.
(42) Yu, C.; Kim, Y. S.; Kim, D.; Grunlan, J. C. *Nano Lett.* **2008**, *8*, 4428.